

Model-Free Optimal Voltage Control via Continuous-Time Zeroth-Order Methods

Xin Chen, Jorge I. Poveda, Na Li

Abstract—In power distribution systems, the growing penetration of renewable energy resources brings new challenges to maintaining voltage safety, which is further complicated by the limited model information of distribution systems. To address these challenges, we develop a model-free optimal voltage control algorithm based on projected primal-dual gradient dynamics and continuous-time zeroth-order method (extreme seeking control). This proposed algorithm i) operates purely based on voltage measurements and does not require any other model information, ii) can drive the voltage magnitudes back to the acceptable range, iii) satisfies the power capacity constraints all the time, iv) minimizes the total operating cost, and v) is implemented in a decentralized fashion where the privacy of controllable devices is preserved and plug-and-play operation is enabled. We prove that the proposed algorithm is semi-globally practically asymptotically stable and is structurally robust to measurement noises. Lastly, the performance of the proposed algorithm is further demonstrated via numerical simulations.

Index Terms—Model-free, voltage control, extremum seeking, projected primal-dual gradient dynamics.

I. INTRODUCTION

Voltage control in a distribution system aims to maintain the voltage magnitudes across the power network within an acceptable range [1]. With rapidly increasing penetration of renewable energy resources, such as photovoltaic (PV) and wind generation, it brings emerging operational challenges to the task of voltage control. On the one hand, the caused reverse power flow may lead to frequent over-voltage issues. On the other hand, large-scale renewable generations introduce significant uncertainty and volatility to the distribution systems, making it much harder to model and control.

There have been a large amount of researches [2]–[8] devoted to voltage control by regulating the slow time-scale devices (such as voltage regulators, shunt capacitors, and on-load-tap-changer transformers) and fast time-scale devices (such as distributed generations (DGs) and static Var compensators (SVCs)). However, most existing voltage control methods are based on power flow models and assume good knowledge of the distribution systems. Therefore, these methods may not perform well when such models and information are absent. References [5]–[8] propose feedback voltage control schemes based on primal-dual gradient methods, dual

ascent approaches, or integral control. Due to the feedback mechanism, these schemes circumvent some of the system information, e.g., real-time uncontrollable power injections, while the distribution network model, such as line parameters and network topology, is still required. In practice, high-accuracy network models and onsite identified network parameters are unavailable for many distribution systems. Moreover, network reconfiguration, line faults, and other operational factors also change the system model from time to time. Hence, it is desirable for the voltage control schemes to operate well in the absence of system models and adapt fast to time-varying operational conditions.

The deployment of smart meters and upgraded communication infrastructures offer an opportunity to overcome these challenges through real-time monitoring and control, which motivates the data-driven voltage control techniques. A type of such data-driven schemes [9]–[11] is to approximate the nonlinear power flow relation with a linear sensitivity model (e.g., the LinDistflow model [7]), and then online estimate the model using measurements and regression methods for voltage control. These schemes generally require a control center to store a large amount of measurement data and solve high-dimensional regression problems in real-time. Reference [12] proposes to reduce the complexity of the linear regression by assuming and exploiting the knowledge of network topology and line resistance-to-reactance ratios. The other type of data-driven schemes is the end-to-end *model-free* control, such as reinforcement learning (RL), which does not explicitly estimate the system model and makes decisions directly based on measurements. A number of recent works [13]–[16] propose to learn voltage control policies using various RL techniques; see review article [17] and references therein for a more comprehensive view. However, applying RL to the control of physical systems is still under development and generally has many limitations, such as safety problems (e.g., physical constraint violation), scalability issues, unstable training process, limited or no theoretical guarantee, etc.

An alternative type of model-free control is based on zeroth-order (or gradient-free) methods [18]. In particular, *extremum seeking* (ES) control [19] is a classic continuous-time zeroth-order optimal control method, which operates using only the output measurements. ES control attracts surging recent attention and has been applied in broad power system applications, including energy consumption control [20], voltage phasor regulation [21], maximum power point tracking [22], etc. Moreover, references [23], [24] develop ES control algorithms to modulate the power injections of distributed energy resources for voltage regulation. In [25], hardware-in-the-loop

X. Chen and N. Li are with the School of Engineering and Applied Sciences, Harvard University, USA; Emails: chen_xin@g.harvard.edu, nali@seas.harvard.edu.

J. I. Poveda is with the Department of Electrical, Computer, and Energy Engineering at the University of Colorado, Boulder, USA; Email: jorge.poveda@colorado.edu.

The work was supported by NSF CNS 1947613, NSF CAREER: ECCS-1553407 and NSF EAGER: ECCS-1839632.

experiments are conducted to verify the viability of a ES-based voltage control scheme. Despite these progresses, one major limitation of existing ES algorithms is that the constraints are not well addressed. Most of the ES methods above consider unconstrained optimization problems for simplicity or penalize the constraint violation in the objective. However, there are various physical constraints, e.g., the power capacity limits, that need to be enforced in practice.

Contributions. In this paper, we study the real-time voltage control through modulating the active and reactive power outputs of fast time-scale controllable devices. To overcome the challenges described above, we develop a model-free optimal voltage control algorithm based on projected primal-dual gradient dynamics (P-PDGD) and ES control. Specifically, by leveraging the structure of P-PDGD, the proposed algorithm can steer the system to an optimal operating point while satisfying the physical constraints. Then ES control is adopted to make this algorithm “model-free” in the sense that the distribution system model is circumvented. The main merits of the proposed algorithm are explained as below:

- 1) (*Optimality*). The proposed algorithm can drive the voltage magnitudes back to the acceptable range while minimizing the total operating cost and always satisfying the power capacity constraints.
- 2) (*Model-Free*). The proposed algorithm is an end-to-end model-free control method that operates purely based on the voltage measurements from the monitored buses. The model information of distribution networks and other power injections is not needed.
- 3) (*Adaptive*). By exploiting real-time measurement, this algorithm is a feedback mechanism that can adapt fast to changes in the dynamical system environment.
- 4) (*Decentralized*). This algorithm is implemented in a decentralized manner, where the privacy of each device can be preserved. Moreover, it allows plug-and-play operation and thus is robust to single/multi-point failures.
- 5) (*Guaranteed Performance*). We mathematically prove the semi-global practical asymptotical stability and the structural robustness (to small measurement noise) of the proposed algorithm, and numerically verify its effectiveness, optimality and robustness via simulations.

To the best of our knowledge, this is the first work on voltage control that unifies all the above features. We also emphasize that the proposed ES-P-PDGD algorithm is a generic model-free method that can be applied to many other multi-agent optimization and control problems. Comparing with existing ES methods, our algorithm can enforce hard physical constraints without sacrificing other performance.

Lastly, we mention a closely-related work [18]. It proposes a model-free primal-dual projected gradient algorithm for real-time optimal power flow based on discrete-time zeroth-order methods, but it makes relatively strong assumptions on the problem setting and lacks explicit convergence results. In contrast, this paper uses and studies the continuous-time ES control dynamics, and provides clear stability guarantee. Besides, distinguished from the projection method used in [18], our algorithm employs the global projection and it leads

to a *Lipschitz continuous* projected dynamical system (see Remark 3), which facilitates the theoretical analysis.

The remainder of this paper is organized as follows: Section II presents the optimal voltage control problem and the preliminaries on ES control. Section III develops the model-free algorithm based on P-PDGD and ES. Section IV analyzes the theoretical performance of the proposed algorithm. Numerical tests are conducted in Section V, and conclusions are drawn in Section VI.

Notations. We use unbolded lower-case letters for scalars, and bolded lower-case letters for column vectors. $\mathbb{R}_+ := [0, +\infty)$ denotes the set of non-negative real values. $|\cdot|$ denotes the cardinality of a set. $\|\cdot\|$ denotes the L2-norm of a vector. $[\mathbf{x}; \mathbf{y}] := [\mathbf{x}^\top, \mathbf{y}^\top]^\top$ denotes the column merge of vectors \mathbf{x}, \mathbf{y} . \blacktriangle highlights the definition of new notations.

II. PROBLEM FORMULATION AND PRELIMINARIES

In this section, we present the formulation of the optimal voltage control problem and introduce the preliminaries on extremum seeking control.

A. Optimal Voltage Control Problem

Consider a distribution network with the monitored bus set \mathcal{M} and the controllable device set \mathcal{C} . Each bus $j \in \mathcal{M}$ has real-time voltage measurement, and the power injection of each device $i \in \mathcal{C}$ can be adjusted for voltage regulation. Depending on the practical system configuration, the controllable devices are flexible to locate at any buses of the distribution network. The optimal voltage control (OVC) problem is formulated as model (1) and explained below:

$$\text{Obj. } \min_{\mathbf{x}} \sum_{i \in \mathcal{C}} c_i(\mathbf{x}_i) \quad (1a)$$

$$\text{s.t. } \mathbf{x}_i \in \mathcal{X}_i, \quad i \in \mathcal{C} \quad (1b)$$

$$\underline{v}_j \leq v_j(\mathbf{x}) \leq \bar{v}_j, \quad j \in \mathcal{M}. \quad (1c)$$

1) *Decision Variable and its Feasible Set:* The decision variable \mathbf{x}_i is the power injection of controllable device $i \in \mathcal{C}$, and its power capacity constraints are described with the feasible set \mathcal{X}_i in (1b). We define

$$\mathbf{x} := (\mathbf{x}_i)_{i \in \mathcal{C}}, \quad \mathcal{X} := \prod_{i \in \mathcal{C}} \mathcal{X}_i.$$

Specifically, we consider the following two types of devices for real-time voltage control with $\mathcal{C} = \mathcal{C}_{\text{svc}} \cup \mathcal{C}_{\text{dg}}$:

i) *Static Var Compensator (SVC)* with the reactive power injection $\mathbf{x}_i := q_i$ and the power capacity constraint (2):

$$\mathcal{X}_i := \{\mathbf{x}_i | \underline{q}_i \leq q_i \leq \bar{q}_i\}, \quad i \in \mathcal{C}_{\text{svc}} \quad (2)$$

where \bar{q}_i and \underline{q}_i are the upper and lower limits, respectively.

ii) *Distributed Generation (DG)* with the active and reactive power injection $\mathbf{x}_i := [p_i, q_i]^\top$ and constraint (3):

$$\mathcal{X}_i := \{\mathbf{x}_i | \underline{p}_i \leq p_i \leq \bar{p}_i, p_i^2 + q_i^2 \leq \bar{s}_i^2\}, \quad i \in \mathcal{C}_{\text{dg}} \quad (3)$$

where \bar{p}_i and \underline{p}_i are the upper and lower limits of active power, and \bar{s}_i denotes the apparent power capacity.

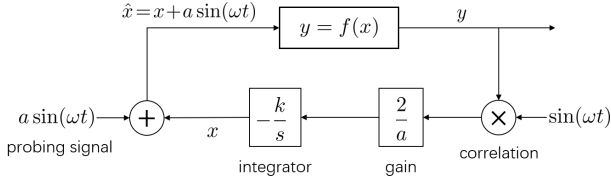


Fig. 1. The block diagram of a simple ES scheme for solving $\min_x f(x)$.

2) *Network and Voltage Constraints*: v_j in (1c) denotes the voltage magnitude at bus $j \in \mathcal{M}$, and \underline{v}_j and \bar{v}_j are the lower and upper voltage limits, respectively. We use the functional form $v_j(\mathbf{x})$ to describe the input-output map from the controllable power injection \mathbf{x} to the voltage magnitude v_j . Essentially, $\mathbf{v}(\mathbf{x}) := (v_j(\mathbf{x}))_{j \in \mathcal{M}}$ captures the nonconvex power flow relation, distribution network model, and other uncontrollable power injections; see [5], [12] for details.

By “system model”, we specifically refer to function $\mathbf{v}(\mathbf{x})$. And “model-free” means that the formulation of $\mathbf{v}(\mathbf{x})$ is unknown and no model estimation is performed for it.

3) *Objective Function*: The objective (1a) aims to minimize the total operating cost with the cost function $c_i(\cdot)$ for each device $i \in \mathcal{C}$. For instance, the quadratic function (4) is a widely used objective [5], [12]:

$$c_i(\mathbf{x}_i) = \begin{cases} c_i^{\text{svc}} \cdot q_i^2, & i \in \mathcal{C}_{\text{svc}} \\ c_{p,i}^{\text{dg}} \cdot p_i^2 + c_{q,i}^{\text{dg}} \cdot q_i^2, & i \in \mathcal{C}_{\text{dg}} \end{cases} \quad (4)$$

where $c_i^{\text{svc}}, c_{p,i}^{\text{dg}}, c_{q,i}^{\text{dg}}$ are the cost coefficients.

We summarize the known and unknown information in our problem setting with the following assumption.

Assumption 1. *The gradient of individual cost function, i.e., $\nabla c_i(\cdot)$, exists and is known to each device $i \in \mathcal{C}$ itself, as well as the feasible set \mathcal{X}_i . The function $\mathbf{v}(\mathbf{x})$ is unknown but the real-time measurement of \mathbf{v} is available.*

Remark 1. In the follows, we consider a general convex cost function $c_i(\cdot)$, while the quadratic cost function (4) is only adopted for simulations. Besides, we assume that the gradient $\nabla c_i(\cdot)$ is known to each device for simplicity. Nevertheless, the proposed voltage control algorithm is applicable to the case when the gradient $\nabla c_i(\cdot)$ is unknown but the cost value c_i can be measured in real time. Similarly, if the real-time measurement of network loss is available, the cost of network loss $l(\mathbf{x})$ can be also included in objective (1a).

B. Preliminaries on Extremum Seeking Control

Extremum seeking (ES) control is a type of model-free control that uses only output feedback to steer a dynamical system to a state where the output function attains an extremum [19]. Therefore, ES can be interpreted as a continuous-time zeroth-order method to solve optimization problems, which essentially estimates the gradient of the objective function based on exploratory probing signals.

Consider the problem of solving $\min_x f(x)$. A straightforward idea is to employ the gradient descent dynamics, i.e., $\dot{x} = -k \cdot \nabla f(x)$. However, this dynamical system is not implementable when the gradient ∇f or the mathematical form

of f is unknown. To address this issue, ES control estimates the gradient $\nabla f(x)$ based on sinusoidal probing signals. The simplest ES scheme that consists of necessary components is shown as Figure 1. Starting from state x , a sinusoidal probing signal $a \sin(\omega t)$ with frequency ω and amplitude a is added to x . Then the perturbed input \hat{x} is fed into the static map $y = f(x)$, and the output y is multiplied by the sinusoidal signal $\sin(\omega t)$, leading to $f(x + a \sin(\omega t)) \sin(\omega t)$. The control loop is closed through the gain $\frac{2}{a}$ and the integrator $\frac{-k}{s}$. Thus the dynamics of this closed-loop feedback ES system can be formulated as

$$\dot{x} = -k \cdot \frac{2}{a} f(x + a \sin(\omega t)) \sin(\omega t), \quad (5)$$

where (a, ω, k) are design parameters.

We first state the fact that the ES dynamics (5) with small a and large ω behaves, approximately, like the gradient descent dynamics $\dot{x} = -k \cdot \nabla f(x)$, which can steer x to a (local) minimum $x^* = \arg \min_x f(x)$ under appropriate conditions on $f(\cdot)$. We also note that to implement the ES dynamics (5), one does not need the knowledge of function f but only its measurement.

The rationale behind is that for sufficiently large value of ω , the ES dynamics (5) exhibits a timescale separation property, where the fast time variation is caused by the sinusoidal signal $\sin(\omega t)$, while the slow variation that is governed by the gain k dominates the evolution of x . By averaging theory, one can obtain a time-invariant average dynamics that describes the main trend of the evolution of x . With small value of a , we consider the following Taylor expansion in the scalar case:

$$f(x + a \sin(\omega t)) = f(x) + a \sin(\omega t) \frac{\partial f(x)}{\partial x} + \mathcal{O}(a^2)$$

Thus the average dynamics of (5) is given by

$$\dot{x} = -k \cdot h_{\text{av}}(x) = -k \cdot \frac{\partial f(x)}{\partial x} + \mathcal{O}(a), \quad (6)$$

where

$$h_{\text{av}}(x) := \frac{1}{T} \int_0^T \frac{2}{a} f(x + a \sin(\omega t)) \sin(\omega t) dt = \frac{\partial f(x)}{\partial x} + \mathcal{O}(a)$$

and $T = \frac{2\pi}{\omega}$. The average dynamics (6) is indeed the gradient descent flow plus a small perturbation $\mathcal{O}(a)$. The same idea can be applied to the multivariate case with an appropriate choice of the (vector) frequencies ω .

The above simple case explains the basic principle of ES control. While a practical ES problem can be much more complex, e.g., involving a plant dynamics, multiple-input and multiple-output, high-pass/low-pass filters, etc. See [19] for a detailed introduction.

Remark 2. The ES system (5) is somehow analogous to the single-point zeroth-order iterative method [26], given by:

$$x_{k+1} = x_k - \eta \frac{1}{r} f(x + ru)u \quad (7)$$

where k is the iteration number, η is the step size, r is the smoothing radius, and u is a random sample from an exploratory distribution, e.g., Gaussian, with zero mean. See [27]–[30] for more studies on the connection between ES control and zeroth-order optimization methods.

III. ALGORITHM DESIGN

In this paper, we aim to design a real-time voltage control algorithm that satisfies the following four requirements:

- 1) **Asymptotic voltage limits.** Once a disturbance occurs, the controller can drive the monitored voltage magnitudes $(v_j)_{j \in \mathcal{M}}$ back to the acceptable interval $[\underline{v}_j, \bar{v}_j]$.
- 2) **Hard capacity constraints.** The power injection \mathbf{x}_i of the controllable device $i \in \mathcal{C}$ should satisfy the physical power capacity constraints \mathcal{X}_i at all times.
- 3) **Optimality.** The controllable devices are regulated in an economically efficient way that minimizes the total operating cost.
- 4) **Model-free.** Information of the power network (topology and line parameters), loads and other power injections is not required.

In this section, we first solve the OVC model (1) with the projected primal-dual gradient dynamics, so that the solution dynamics can be interpreted as the voltage controller which meets the first three requirements above. Then we take the fourth requirement into account and develop a model-free voltage control algorithm based on ES control.

A. Projected Primal-Dual Gradient Dynamics

We make the following two standard assumptions on the OVC model (1) to render it a convex optimization problem with strong duality. We emphasize that these assumptions are mainly for theoretical analysis, and the proposed control algorithm can be applied to power systems with a nonlinear power flow model, which is validated by our simulations.

Assumption 2. For all $i \in \mathcal{C}$, the function $c_i(\cdot)$ is convex and has locally Lipschitz gradients, and the set \mathcal{X}_i is closed and convex. Also, the function $v_j(\cdot)$ is affine for all $j \in \mathcal{M}$.

Assumption 3. The OVC problem (1) has a finite optimum, and the Slater's conditions hold for the problem (1).

We employ the projected primal-dual gradient dynamics (**P-PDGD**) method to solve the OVC model (1). With dual variables $\boldsymbol{\lambda}^+ := (\lambda_j^+)_{j \in \mathcal{M}}$, $\boldsymbol{\lambda}^- := (\lambda_j^-)_{j \in \mathcal{M}}$, the saddle point problem of the OVC model (1) is formulated as

$$\begin{aligned} \max_{\boldsymbol{\lambda} \geq 0} \min_{\mathbf{x} \in \mathcal{X}} L(\mathbf{x}, \boldsymbol{\lambda}) &= \sum_{i \in \mathcal{C}} c_i(\mathbf{x}_i) \\ &+ \sum_{j \in \mathcal{M}} \left[\lambda_j^+ (v_j(\mathbf{x}) - \bar{v}_j) + \lambda_j^- (\underline{v}_j - v_j(\mathbf{x})) \right] \end{aligned} \quad (8)$$

where $\boldsymbol{\lambda} := [\boldsymbol{\lambda}^+; \boldsymbol{\lambda}^-]$ and $L(\mathbf{x}, \boldsymbol{\lambda})$ denotes the Lagrangian function. Then we solve problem (8) with P-PDGD (9):

$$\dot{\mathbf{x}}_i = k_x \left[\text{Proj}_{\mathcal{X}_i} \left(\mathbf{x}_i - \alpha_x \frac{\partial L(\mathbf{x}, \boldsymbol{\lambda})}{\partial \mathbf{x}_i} \right) - \mathbf{x}_i \right], i \in \mathcal{C} \quad (9a)$$

$$\dot{\lambda}_j^+ = k_\lambda \left[\text{Proj}_{\mathbb{R}_+} \left(\lambda_j^+ + \alpha_\lambda \frac{\partial L(\mathbf{x}, \boldsymbol{\lambda})}{\partial \lambda_j^+} \right) - \lambda_j^+ \right], j \in \mathcal{M} \quad (9b)$$

$$\dot{\lambda}_j^- = k_\lambda \left[\text{Proj}_{\mathbb{R}_+} \left(\lambda_j^- + \alpha_\lambda \frac{\partial L(\mathbf{x}, \boldsymbol{\lambda})}{\partial \lambda_j^-} \right) - \lambda_j^- \right], j \in \mathcal{M} \quad (9c)$$

where $k_x, k_\lambda, \alpha_x, \alpha_\lambda$ are positive parameters, and the Lipschitz projection operator $\text{Proj}_{\mathcal{X}}(\cdot)$ is defined as

$$\text{Proj}_{\mathcal{X}}(\mathbf{x}) := \underset{\mathbf{y} \in \mathcal{X}}{\text{argmin}} \|\mathbf{y} - \mathbf{x}\|. \quad (10)$$

The gradients in (9) are given by

$$\frac{\partial L(\mathbf{x}, \boldsymbol{\lambda})}{\partial \mathbf{x}_i} = \nabla c_i(\mathbf{x}_i) + \sum_{j \in \mathcal{M}} (\lambda_j^+ - \lambda_j^-) \frac{\partial v_j(\mathbf{x})}{\partial \mathbf{x}_i} \quad (11a)$$

$$\frac{\partial L(\mathbf{x}, \boldsymbol{\lambda})}{\partial \lambda_j^+} = v_j(\mathbf{x}) - \bar{v}_j \quad (11b)$$

$$\frac{\partial L(\mathbf{x}, \boldsymbol{\lambda})}{\partial \lambda_j^-} = \underline{v}_j - v_j(\mathbf{x}). \quad (11c)$$

▲ Denote $\mathbf{z} := [\mathbf{x}; \boldsymbol{\lambda}]$ and define $\mathcal{Z} := \mathcal{X} \times \mathbb{R}_+^{2|\mathcal{M}|}$ as the feasible set of \mathbf{z} in (9).

Remark 3. (*Projection of Dynamical System*) The projection method used in (9) is referred as *global projection* [31]. By [31, Lemma 3], it ensures that $\mathbf{z}(t) \in \mathcal{Z}$ for all time $t \geq 0$ when the initial condition $\mathbf{z}(0) \in \mathcal{Z}$. For example, consider the dynamics of \mathbf{x}_i . The intuition of this type of projection is that (9a) attempts to take a step forward with stepsize α_x along the gradient descent direction, then checks whether the arrival point $\mathbf{x}_i - \alpha_x \frac{\partial L(\mathbf{x}, \boldsymbol{\lambda})}{\partial \mathbf{x}_i}$ is feasible to \mathcal{X}_i . If feasible, (9a) reduces to the ordinary gradient descent dynamics $\dot{\mathbf{x}}_i = -k_x \alpha_x \frac{\partial L(\mathbf{x}, \boldsymbol{\lambda})}{\partial \mathbf{x}_i}$, otherwise a projection is performed to guarantee the feasibility of \mathbf{x}_i . Note that the P-PDGD (9) is Lipschitz continuous; it differs from other types of discontinuous projections considered in literature, e.g., [18], [32], [33], which project the dynamics onto the tangent cone of the feasible set, and thus they need the sophisticated analysis tools for discontinuous dynamical systems.

Following the P-PDGD (9), the state $\mathbf{x}(t)$ will remain within the feasible set \mathcal{X} and converge to a steady-state operating point that is an optimal solution of the OVC problem (1). This is restated formally as Theorem 1.

Theorem 1. (*Global Asymptotical Stability.*) Under Assumption 2 and 3, with initial condition $\mathbf{z}(0) \in \mathcal{Z}$, the trajectory $\mathbf{z}(t)$ of the P-PDGD (9) will stay within \mathcal{Z} for all $t \geq 0$ and globally asymptotically converge to an optimal solution $\mathbf{z}^* := [\mathbf{x}^*; \boldsymbol{\lambda}^*]$ of the saddle point problem (8), where \mathbf{x}^* is an optimal solution of the OVC problem (1).

The proof of Theorem 1 mainly follows the asymptotical stability of globally projected (primal-dual) dynamical systems [34, Lemma 2.4] [31]. A detailed proof is provided in Appendix A. As a result, the P-PDGD (9) can be regarded as the voltage control mechanism that meets the first three requirements above. In the next subsection, we will take into account the fourth requirement and develop a model-free control algorithm based on the proposed P-PDGD (9).

B. Model-Free Voltage Control Algorithm

The P-PDGD (9) cannot be implemented without knowledge of the system model $\mathbf{v}(\mathbf{x})$. Note that there are two occasions in the P-PDGD (9) where this model is needed:

- 1) The gradients $\frac{\partial v_j(\mathbf{x})}{\partial \mathbf{x}_i}$ in (11a) for $i \in \mathcal{C}, j \in \mathcal{M}$;
- 2) The functions $v_j(\mathbf{x})$ in (11b) (11c) for $j \in \mathcal{M}$.

To develop a model-free controller, we propose the following two strategies accordingly:

Strategy 1): Use ES control to “estimate” the gradients $\frac{\partial v_j(\mathbf{x})}{\partial \mathbf{x}_i}$ for all $i \in \mathcal{C}, j \in \mathcal{M}$.

Strategy 2): Substitute the function $v_j(\cdot)$ by the real-time voltage measurement $v_j^{\text{mea}}(t)$ for all $j \in \mathcal{M}$.

To implement Strategy 1), we add a small sinusoidal probing signal to each power injection with

$$\hat{\mathbf{x}}_i(t) = \mathbf{x}_i(t) + a \sin(\omega_i t), \quad i \in \mathcal{C} \quad (12)$$

where a is the small amplitude¹ and the sinusoidal signal is

$$\sin(\omega_i t) := \begin{cases} \sin(\omega_i t), & i \in \mathcal{C}_{\text{svc}} \\ [\sin(\omega_i^p t), \sin(\omega_i^q t)]^\top, & i \in \mathcal{C}_{\text{dg}}. \end{cases} \quad (13)$$

▲ Let $N = |\mathcal{C}_{\text{svc}}| + 2|\mathcal{C}_{\text{dg}}|$ be the dimensionality of the decision variable \mathbf{x} . Define $\sin(\omega t) := (\sin(\omega_i t))_{i \in \mathcal{C}} \in \mathbb{R}^N$ as the column vector that collects all the sinusoidal signals. The frequencies $\omega := (\omega_i)_{i \in \mathcal{C}}$ are selected as

$$\omega_n = \frac{2\pi}{\varepsilon_\omega} \kappa_n, \quad \forall n \in [N] := \{1, \dots, N\} \quad (14)$$

where ε_ω is a small positive parameter and $\kappa_i \neq \kappa_j$ for all $i \neq j$ are rational numbers. In this way, each element x_n in \mathbf{x} is assigned with a particular frequency ω_n .

Based on the above description, the P-PDGD (9) is modified as the **ES-P-PDGD** (15):

$$\dot{\mathbf{x}}_i = k_x \left[\text{Proj}_{\hat{\mathcal{X}}_i}(\mathbf{x}_i - \alpha_x \mathbf{h}_i(\mathbf{x}_i, \boldsymbol{\lambda}, \boldsymbol{\xi}_i^j)) - \mathbf{x}_i \right], \quad i \in \mathcal{C} \quad (15a)$$

$$\dot{\lambda}_j^+ = k_\lambda \left[\text{Proj}_{\mathbb{R}_+}(\lambda_j^+ + \alpha_\lambda (\mu_j - \bar{v}_j)) - \lambda_j^+ \right], \quad j \in \mathcal{M} \quad (15b)$$

$$\dot{\lambda}_j^- = k_\lambda \left[\text{Proj}_{\mathbb{R}_+}(\lambda_j^- + \alpha_\lambda (\underline{v}_j - \mu_j)) - \lambda_j^- \right], \quad j \in \mathcal{M} \quad (15c)$$

$$\dot{\boldsymbol{\xi}}_i^j = \frac{1}{\epsilon} \left[-\boldsymbol{\xi}_i^j + \frac{2}{a} v_j(\hat{\mathbf{x}}(t)) \sin(\omega_i t) \right], \quad j \in \mathcal{M}, i \in \mathcal{C} \quad (15d)$$

$$\dot{\mu}_j = \frac{1}{\epsilon} \left[-\mu_j + v_j(\hat{\mathbf{x}}(t)) \right], \quad j \in \mathcal{M} \quad (15e)$$

where ϵ is a small positive parameter, and

$$\hat{\mathbf{x}}(t) := \mathbf{x}(t) + a \sin(\omega t) \quad (16a)$$

$$\mathbf{h}_i(\mathbf{x}_i, \boldsymbol{\lambda}, \boldsymbol{\xi}_i^j) := \nabla c_i(\mathbf{x}_i) + \sum_{j \in \mathcal{M}} (\lambda_j^+ - \lambda_j^-) \boldsymbol{\xi}_i^j. \quad (16b)$$

The key difference between P-PDGD (9) and ES-P-PDGD (15) is the introduction of new variables $\boldsymbol{\xi} := (\boldsymbol{\xi}_i^j)_{j \in \mathcal{M}, i \in \mathcal{C}}$ and $\boldsymbol{\mu} := (\mu_j)_{j \in \mathcal{M}}$. We explain the rationale and benefits of this modification with Remark 4. To ensure the actual power injection $\hat{\mathbf{x}}_i \in \mathcal{X}_i$, we replace \mathcal{X}_i with the shrunken feasible set $\hat{\mathcal{X}}_i$ (17) in (15a). As $a \rightarrow 0^+$, $\hat{\mathcal{X}}$ recovers to \mathcal{X} .

$$\hat{\mathcal{X}}_i := \begin{cases} \underline{q}_i + a \leq q_i \leq \bar{q}_i - a, & i \in \mathcal{C}_{\text{svc}} \\ \underline{p}_i + a \leq p_i \leq \bar{p}_i - a, p_i^2 + q_i^2 \leq (\bar{s}_i - \sqrt{2}a)^2, & i \in \mathcal{C}_{\text{dg}}. \end{cases} \quad (17)$$

Remark 4. (*Fast Dynamics of $\boldsymbol{\xi}$ and $\boldsymbol{\mu}$.*) In essence, $\boldsymbol{\xi}_i^j$ and μ_j are the real-time approximations of the gradient $\frac{\partial v_i}{\partial \mathbf{x}_i}$ and the value v_j , respectively. The intuition behind is that by setting ϵ sufficiently small, the dynamics of $\boldsymbol{\xi}_i^j$ and μ_j , i.e., (15d) (15e), operate in a faster time scale compared to the dynamics

¹For notational simplicity, we adopt an identical amplitude a for all power injections here. In practice, different amplitude parameters can be used.

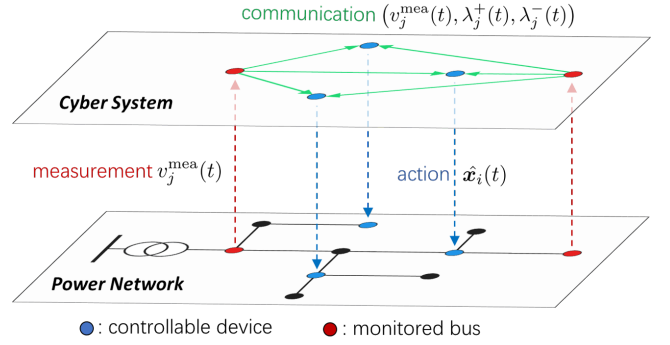


Fig. 2. Schematic of the proposed MF-OVC mechanism.

of $(\mathbf{x}, \boldsymbol{\lambda})$. The advantages of introducing these fast dynamics of $\boldsymbol{\xi}$ and $\boldsymbol{\mu}$ include:

- 1) It facilitates the analysis of the algorithm via averaging theory, since the time-varying sinusoidal signals do not appear inside the projection operators. Moreover, the fast dynamics are linear, which can be easily handled by singular perturbation theory.
- 2) The fast dynamics (15d) (15e) can be seen as low-pass filters, which can diminish the oscillations and improve the transient performance of the closed-loop system.

Since $\hat{\mathbf{x}}(t)$ is the actual power injection to the physical system at time t , we can substitute $v_j(\hat{\mathbf{x}})$ with the voltage measurement $v_j^{\text{mea}}(t)$ in (15), i.e., Strategy 2). Consequently, we develop the model-free optimal voltage control (**MF-OVC**) algorithm as Algorithm 1, which is indeed the ES-P-PDGD (15) with the measurement substitution.

Algorithm 1 Model-Free Optimal Voltage Control (MF-OVC) Algorithm.

At every time t , perform the following steps:

- **Each monitored bus** $j \in \mathcal{M}$ measures the local voltage magnitude $v_j^{\text{mea}}(t)$, updates $(\lambda_j^+, \lambda_j^-, \mu_j)$ according to

$$\text{Equations (15b) (15c)} \quad (18a)$$

$$\dot{\mu}_j = \frac{1}{\epsilon} \left[-\mu_j + v_j^{\text{mea}}(t) \right] \quad (18b)$$

and broadcasts $(v_j^{\text{mea}}(t), \lambda_j^+(t), \lambda_j^-(t))$ to every controllable device $i \in \mathcal{C}$.

- **Each controllable device** $i \in \mathcal{C}$ updates $(\mathbf{x}_i, \boldsymbol{\xi}_i^j)$ by

$$\text{Equation (15a)} \quad (19a)$$

$$\dot{\boldsymbol{\xi}}_i^j = \frac{1}{\epsilon} \left[-\boldsymbol{\xi}_i^j + \frac{2}{a} v_j^{\text{mea}}(t) \sin(\omega_i t) \right], \quad j \in \mathcal{M} \quad (19b)$$

and executes power injection $\hat{\mathbf{x}}_i(t) = \mathbf{x}_i(t) + a \sin(\omega_i t)$.

The implementation of the proposed MF-OVC algorithm is illustrated in Figure 2. Each monitored bus $j \in \mathcal{M}$ measures its local voltage magnitude v_j^{mea} from the physical layer, then updates $(\mu_j, \lambda_j^+, \lambda_j^-)$ and communicates $(v_j^{\text{mea}}, \lambda_j^+, \lambda_j^-)$ in the cyber layer. Each controllable device $i \in \mathcal{C}$ updates $(\boldsymbol{\xi}_i^j, \mathbf{x}_i)$ based on the received information, and the power injection command $\hat{\mathbf{x}}_i$ is executed in the physical layer. Then

the power network responses to the power injection $\hat{\mathbf{x}}$ and presents the corresponding voltage profiles $\mathbf{v}(\hat{\mathbf{x}})$. This forms a closed-loop feedback control system. Although the MF-OVC algorithm is developed based on a static OVC problem (1), it can adapt fast to dynamical system environments and handle voltage violation under time-varying power disturbances, due to the feedback mechanism and exploitation of real-time measurements. This is validated by the simulations in Section V-C. As a result, the proposed algorithm unifies all the merits described in the introduction section.

IV. PERFORMANCE ANALYSIS

This section presents the theoretical analysis on the performance of the proposed MF-OVC algorithm. In particular, we focus on the ES-P-PDGD (15) and study its stability properties as well as its robustness to measurement noises.

A. Stability Analysis of ES-P-PDGD

▲ Denote $\mathbf{z} := [\mathbf{x}; \boldsymbol{\lambda}]$ and $\hat{\mathcal{X}} := \prod_{i \in \mathcal{C}} \hat{\mathcal{X}}_i$. Let $\hat{\mathcal{Z}} := \hat{\mathcal{X}} \times \mathbb{R}_+^{2|\mathcal{M}|}$ be the feasible set of \mathbf{z} in the ES-P-PDGD (15), and $K := (2|\mathcal{C}_{\text{dg}}| + |\mathcal{C}_{\text{svc}}| + 1)|\mathcal{M}|$ be the dimensionality of $[\boldsymbol{\xi}; \boldsymbol{\mu}]$. Denote $\hat{\mathcal{A}}$ as the saddle point set for the saddle point problem (8) with $\hat{\mathcal{X}}$, i.e., any point $\hat{\mathbf{z}}^* \in \hat{\mathcal{A}}$ is an optimal solution of (8) with $\hat{\mathcal{X}}$.² Denote the distance between \mathbf{z} and $\hat{\mathcal{A}}$ as

$$\|\mathbf{z}\|_{\hat{\mathcal{A}}} := \inf_{\boldsymbol{\alpha} \in \hat{\mathcal{A}}} \|\mathbf{z} - \boldsymbol{\alpha}\|.$$

Definition 1. A continuous function $\beta(r, t) : \mathbb{R}_+ \times \mathbb{R}_+ \rightarrow \mathbb{R}_+$ is said to be of class- \mathcal{KL} if it is zero at zero and strictly increasing in the first argument r , and non-increasing in the second argument t and converging to zero as $t \rightarrow +\infty$.

The stability of ES-P-PDGD (15) is stated as Theorem 2.

Theorem 2. (Semi-Global Practical Asymptotical Stability.) Suppose that the saddle point set $\hat{\mathcal{A}}$ is compact. Under Assumption 2 and 3, there exists a class- \mathcal{KL} function β such that for any compact set $\mathcal{D} \subset \hat{\mathcal{Z}} \times \mathbb{R}^K$ of initial condition, and any desired precision $\nu > 0$, there exists $\epsilon^* > 0$ such that for any $\epsilon \in (0, \epsilon^*)$, there exists $a^* > 0$ such that for any $a \in (0, a^*)$, there exists $\epsilon_\omega^* > 0$ such that for any $\epsilon_\omega \in (0, \epsilon_\omega^*)$, the trajectory $\mathbf{z}(t)$ of the ES-P-PDGD (15) satisfies

$$\|\mathbf{z}(t)\|_{\hat{\mathcal{A}}} \leq \beta(\|\mathbf{z}(0)\|_{\hat{\mathcal{A}}}, t) + \nu, \quad \forall t \geq 0. \quad (20)$$

We prove Theorem 2 using averaging theory and singular perturbation theory [35], [36]. The detailed proof of Theorem 2 is provided in Appendix B.

Remark 5. We explain the key observations of Theorem 2 as follows:

- Due to the small probing sinusoidal signals $a \sin(\omega t)$ in the ES-P-PDGD (15), the state \mathbf{z} will not converge to a fixed point anymore, but rather to a small ν -neighborhood of $\hat{\mathcal{A}}$. This property is described by the bound (20). By setting the parameters $(\epsilon, a, \epsilon_\omega)$ sufficiently small, one can make this precision ν as small as desired.

²Here, the notations with “ \wedge ” on the head represent the counterparts with the feasible set $\hat{\mathcal{X}}$.

- As $(\epsilon, a, \epsilon_\omega) \rightarrow 0^+$, the ES-P-PDGD (15) recovers the same convergence rate of the P-PDGD (9), as indicated in the proof of Theorem 2.

- As stated in Theorem 2, the tuning order of parameters is relevant: first set ϵ sufficiently small, then a , and lastly ϵ_ω . This order comes mainly from the proof and can guide us on how to tune these parameters in practice.

Remark 6. We note that the assumption of a compact saddle point set $\hat{\mathcal{A}}$ in Theorem 2 is standard for the application of averaging theory and singular perturbation theory. For the OVC problem (1), if the cost function $c_i(\cdot)$ is strictly convex for all $i \in \mathcal{C}$ and the Jacobian matrix $\nabla_{\mathbf{x}} \mathbf{v}(\mathbf{x})$ is of full row rank, one can prove that the saddle point set $\hat{\mathcal{A}}$ is singleton, i.e., the optimal solution of the saddle point problem (8) is *unique*, by [37, Proposition 1]. In practice, the condition that the Jacobian matrix $\nabla_{\mathbf{x}} \mathbf{v}(\mathbf{x})$ is of full row rank can be satisfied when the number of controllable devices is more than the monitored buses in the distribution system [38].

B. Robustness to Measurement Noise

The proposed algorithm purely relies on the voltage measurement for control. Accordingly, the following corollary of Theorem 2 [39] indicates that this algorithm is robust to *small* additive state measurement noise. Moreover, the numerical simulations in Section V-D verify the robustness even when the noise is relatively large.

Corollary 1. (Structural Robustness.) For any tuple of $(\epsilon, a, \epsilon_\omega)$ that induces the bound (20), under the same conditions in Theorem 2, there exists $\rho^* > 0$ such that for any measurement noise $\mathbf{d} : \mathbb{R}_+ \rightarrow \mathbb{R}^{|\mathcal{M}|}$ with $\sup_{t \geq 0} \|\mathbf{d}(t)\| \leq \rho^*$, the trajectory $\mathbf{z}(t)$ of the ES-P-PDGD (15) with additive state measurement noise \mathbf{d} satisfies

$$\|\mathbf{z}(t)\|_{\hat{\mathcal{A}}} \leq \beta(\|\mathbf{z}(0)\|_{\hat{\mathcal{A}}}, t) + 2\nu, \quad \forall t \geq 0. \quad (21)$$

Comparing with (20), the ES-P-PDGD (15) with small additive measurement noise \mathbf{d} maintains similar convergence results, and noise \mathbf{d} leads to an additional ν term in (21). Besides, this robustness property can be extended to other small additive perturbations.

V. NUMERICAL SIMULATIONS

In this section, we demonstrate the performance of the proposed MF-OVC algorithm via numerical simulations. Specifically, we test the MF-OVC algorithm under step and continuous power disturbances. The impact of noises in voltage measurements is studied numerically as well.

A. Simulation Setup

The modified PG&E 69-bus distribution system, shown as Figure 3, is used as the test system. There are three PV plants at bus 35, 54 and 69, which operate in the maximum power point tracking mode. The controllable devices include three SVCs (located at bus 35, 42 and 67) and three DGs (located at bus 20, 40, 50). Their power capacity limits are set to

$$q_i = -1.5 \text{ MVar}, \quad \bar{q}_i = 0.6 \text{ MVar}, \quad i \in \mathcal{C}_{\text{svc}}$$

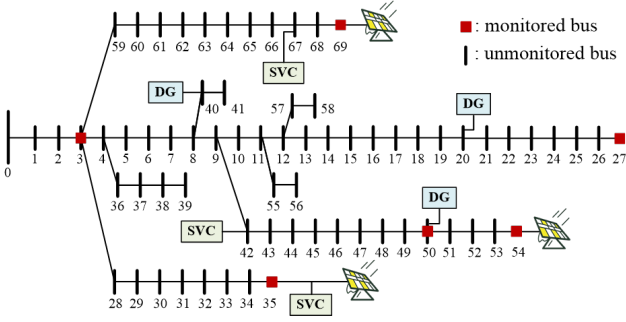


Fig. 3. The modified PG&E 69-bus distribution feeder.

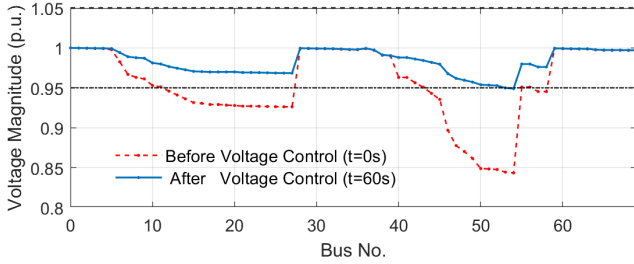


Fig. 4. The voltage magnitude profiles before and after voltage control (black dotted lines: upper (1.05 p.u.) and lower (0.95 p.u.) voltage limits).

$$\bar{p}_i = 0 \text{ MW}, \bar{p}_i = 1.5 \text{ MW}, \bar{s}_i = 1.8 \text{ MVA}, \quad i \in \mathcal{C}_{\text{dg}}.$$

We select bus 3, 27, 35, 50, 54 and 69 as the monitored buses. The voltage of bus 0 (slack bus) is 10.5 kV (1 p.u.), and the lower and upper bounds of voltage magnitude are set as 0.95 p.u. and 1.05 p.u., respectively. We use the quadratic cost function (4) with the coefficient $c_i^{\text{svc}} = 0.1, c_{p,i}^{\text{dg}} = 1, c_{q,i}^{\text{dg}} = 0.5$. For the MF-OVC algorithm, we set $a = 0.05, \epsilon = 0.02, \epsilon_\omega = 0.05$, and $\kappa_n = 2n - 1$ for $n = 1, \dots, 9$.

Although an affine voltage function $v(\mathbf{x})$ is assumed for theoretical analysis, we perform all the simulations based on a *full nonconvex AC power flow model* using the Matpower software [40].

B. Static Voltage Control Under Step Power Change

Consider the test scenario when the three PV plants are suddenly shut down at time $t = 0$ and all loads remain fixed. Due to the curtailment of PV generation and heavy loads, the voltage profiles of the test system decrease to a low level. It leads to voltage violation at many buses, shown as the red dashed curve in Figure 4. We ran the proposed MF-OVC algorithm for voltage regulation from the start time $t = 0$. The simulation results are shown as Figure 5 and Figure 6.

From Figure 5, it is observed that the proposed MF-OVC algorithm can quickly bring the voltage magnitudes of monitored buses back to the acceptable range. The small high-frequency oscillations in voltage are caused by the exploratory sinusoidal signals in the MF-OVC algorithm. As a result, the voltage profiles of the entire test system were restored to the acceptable level (see the blue curve in Figure 4), due to the selection of representative monitored buses. Figure 6 illustrates the dynamics of the power outputs of DGs and SVCs. It is seen

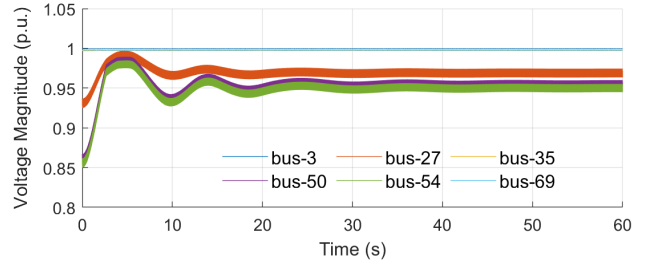


Fig. 5. Voltage dynamics of the monitored buses under step power change.

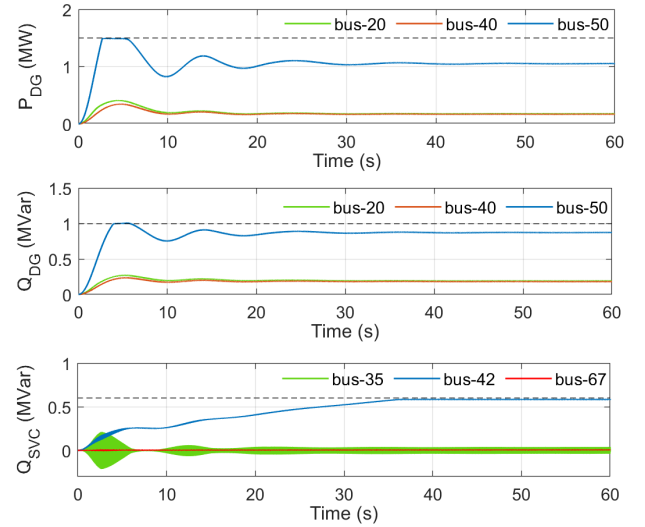


Fig. 6. The active/reactive power outputs of DGs and SVCs (black dashed lines: the corresponding power capacity limits).

that the power outputs converge to fixed values (with small oscillations) within tens of seconds, and the power capacity constraints are satisfied all the time. Besides, we solve the OVC model (1) to obtain the optimal solution \mathbf{x}^* ³, which turns out to be the converged values in Figure 6. It verifies the optimality of the MF-OVC algorithm.

C. Dynamic Voltage Control Under Continuous Change

We then test the performance of the proposed MF-OVC algorithm under time-varying loads and PV generations. We add a 10% random perturbation to the total load, and a real-world PV generation profile, shown as Figure 7, is applied to the three PV plants in the test system. We ran the proposed MF-OVC algorithm for voltage regulation and compared it with the case without voltage control.

The simulation results are illustrated in Figure 8. In the absence of voltage control, the test system violates the lower voltage limit (0.95 p.u.) when the PV generation is low, and the upper voltage limit (1.05 p.u.) when the PV generation is high. In contrast, the proposed MF-OVC algorithm can effectively adapt to the continuous power disturbances and maintain the voltage profiles within the acceptable range.

³We solve the OVC model (1) with the CVX package [41], and the linearized Distflow model [5] is used as the power flow model for $v(\mathbf{x})$.

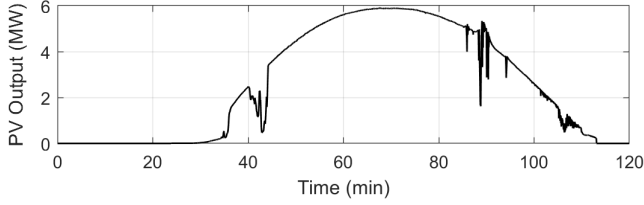


Fig. 7. The time-varying total PV generation over two hours.

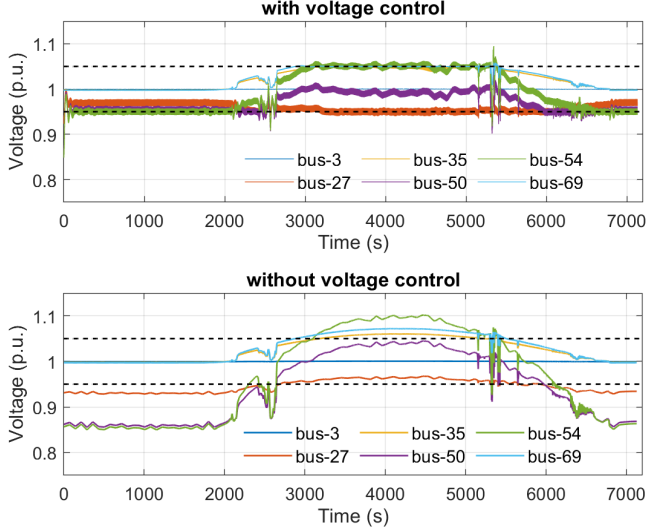


Fig. 8. Voltage dynamics of the monitored buses under continuous power disturbances (black dashed lines: upper (1.05 p.u.) and lower (0.95 p.u.) voltage limits).

D. Impact of Measurement Noise

To study the impact of measurement noises, we consider the noisy voltage measurement $\tilde{v}_j^{\text{mea}}(t)$, whose deviation from the base voltage value (1 p.u.) follows (22):

$$\tilde{v}_j^{\text{mea}}(t) - 1 = (v_j(\mathbf{x}(t)) - 1) \times (1 + \delta_j(t)) \quad (22)$$

where $v_j(\mathbf{x}(t))$ denotes the true voltage magnitude, and δ_j is the perturbation ratio. We assume that δ_j is a Gaussian random variable with $\delta_j \sim \mathcal{N}(0, \sigma^2)$, which is independent across time t and other monitored buses. We tune the standard deviation σ from 0.1 to 0.5 to simulate different levels of noises and test the performance of the MF-OVC algorithm under step power changes. The simulation results are shown as Figure 9, and the noiseless case with $\sigma = 0$ is illustrated in Figure 5. As expected, larger noise amplitudes lead to higher oscillations in the voltage dynamics. While the MF-OVC algorithm is robust to the voltage measurement noises and can bring the voltage profiles back to the acceptable interval in all the cases.

VI. CONCLUSION

In this paper, we developed a real-time model-free optimal voltage control algorithm based on projected primal-dual gradient dynamics and extremum seeking control. The proposed algorithm operates purely based on the voltage measurement and does not require any other network information. With appropriate parameters, this algorithm can effectively bring the

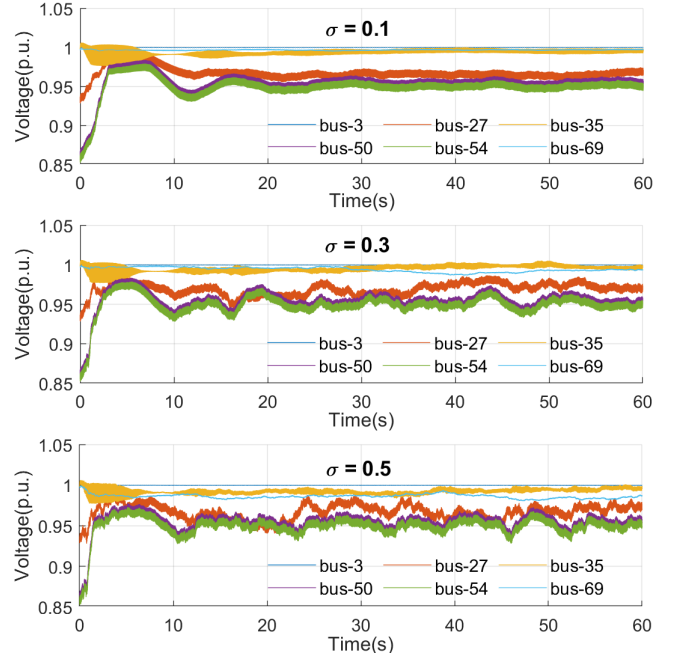


Fig. 9. Voltage dynamics of the monitored buses with noisy voltage measurements.

monitored voltage magnitudes back to the acceptable range with minimum operational cost, while respecting the power capacity constraints all the time. Numerical simulations on a modified PG&E 69-bus distribution feeder demonstrated that the proposed algorithm is capable of handling voltage violation under step or continuous power disturbances, and is robust to measurement noises.

APPENDIX

A. Proof of Theorem 1

We first have the result of the following Proposition 1 that connects the saddle point problem (8) and the P-PDGD (9). This proposition can be proved by checking the KKT conditions of (8) and using [42, Theorem 3.25].

Proposition 1. *The optimal solutions of the saddle point problem (8) are equivalent to the equilibrium points of the P-PDGD (9).*

We then study the stability properties of the P-PDGD (9). Denote $\mathbf{z} := [\mathbf{x}; \boldsymbol{\lambda}]$, and let $\mathbf{z}^* := [\mathbf{x}^*; \boldsymbol{\lambda}^*]$ be the optimal solution of (8). Define the mapping

$$H(\mathbf{z}) := [\nabla_{\mathbf{x}} L(\mathbf{x}, \boldsymbol{\lambda}); -\nabla_{\boldsymbol{\lambda}} L(\mathbf{x}, \boldsymbol{\lambda})],$$

where $L(\mathbf{x}, \boldsymbol{\lambda})$ is the Lagrangian function in (8). The P-PDGD (9) can be written in compact form⁴ as:

$$\dot{\mathbf{z}} = \text{Proj}_{\mathcal{Z}}(\mathbf{z} - \alpha H(\mathbf{z})) - \mathbf{z} := \mathbf{f}(\mathbf{z}), \quad (23)$$

where $\mathcal{Z} := \mathcal{X} \times \mathbb{R}_+^{2|\mathcal{M}|}$. Since $\text{Proj}_{\mathcal{Z}}(\cdot)$ is a singleton and Lipschitz on $\mathbb{R}^{|\mathcal{Z}|}$ with constant $L = 1$ [43, Proposition 2.4.1], the dynamics $\mathbf{f}(\mathbf{z})$ in (23) is locally Lipschitz on \mathcal{Z}

⁴Without loss of generality, we set the time constant $k = 1$ for simplicity.

by Assumption 2. Moreover, by [31, Lemma 3], we have that $z(t) \in \mathcal{Z}$ for all time $t \geq 0$ whenever $z(0) \in \mathcal{Z}$.

Next, consider the following Lyapunov function V :

$$\begin{aligned} V(z) &:= \frac{1}{2} \|z - z^*\|^2 + L(x, \lambda^*) - L(x^*, \lambda) \\ &= \frac{1}{2} \|z - z^*\|^2 + L(x, \lambda^*) - L(x^*, \lambda^*) \\ &\quad + L(x^*, \lambda^*) - L(x^*, \lambda) \geq \frac{1}{2} \|z - z^*\|^2. \end{aligned} \quad (24)$$

The time derivative of V along the P-PDGD (9) is

$$\dot{V}(z) = \nabla_z V(z)^\top \dot{z} = (z - z^* + H(z))^\top f(z). \quad (25)$$

One useful property is stated as Lemma 1.

Lemma 1. *For any $\alpha > 0$, we have*

$$(z - z^* + \alpha H(z))^\top f(z) \leq -\|f(z)\|^2 - \alpha(z - z^*)^\top H(z).$$

The proof of Lemma 1 follows [34, Lemma 2.4]. For completeness, here we provide a detailed proof as the three steps below:

1) We use the fact [32] that the projection operator satisfies

$$(\text{Proj}_{\mathcal{Z}}(\gamma) - \beta)^\top (\gamma - \text{Proj}_{\mathcal{Z}}(\gamma)) \geq 0, \quad (26)$$

for all $\gamma \in \mathbb{R}^{|\mathcal{Z}|}$, $\beta \in \mathcal{Z}$.

2) Let $\gamma = z - \alpha H(z)$ and $\beta = z^*$, then (26) becomes

$$(f(z) + z - z^*)^\top (\alpha H(z) + f(z)) \leq 0. \quad (27)$$

3) Thus we obtain Lemma 1 by

$$\begin{aligned} &(z - z^* + \alpha H(z))^\top f(z) \\ &= (-f(z) + f(z) + z - z^* + \alpha H(z))^\top f(z) \\ &= -\|f(z)\|^2 + (f(z) + z - z^*)^\top f(z) + \alpha H(z)^\top f(z) \\ &\leq -\|f(z)\|^2 - \alpha(f(z) + z - z^*)^\top H(z) + \alpha H(z)^\top f(z) \\ &= -\|f(z)\|^2 - \alpha(z - z^*)^\top H(z) \end{aligned}$$

where the inequality above is because of (27).

Using the result of Lemma 1 with $\alpha = 1$, we obtain

$$\begin{aligned} \dot{V}(z) &\leq -\|f(z)\|^2 - (z - z^*)^\top H(z) \\ &= -\|f(z)\|^2 - (x - x^*)^\top \nabla_x L(x, \lambda) + (\lambda - \lambda^*)^\top \nabla_\lambda L(x, \lambda) \\ &\leq -\|f(z)\|^2 + L(x^*, \lambda) - L(x, \lambda) + L(x, \lambda) - L(x, \lambda^*) \\ &= -\|f(z)\|^2 + L(x^*, \lambda) - L(x^*, \lambda^*) + L(x^*, \lambda^*) - L(x, \lambda^*) \\ &\leq -\|f(z)\|^2 \leq 0 \end{aligned} \quad (28)$$

where the second inequality follows that $L(x, \lambda)$ is convex in x and concave in λ .

By (28), we have that every compact level set of V is forward invariant, and since V is radially unbounded, it follows that all trajectories $z(t)$ remain bounded. Thus, by LaSalle's Theorem [35, Theorem 4.4], $z(t)$ converges to the largest invariant compact subset \mathcal{M} contained in \mathcal{S} :

$$\mathcal{S} := \{z \in \mathcal{Z} : \dot{V}(z) = 0, V(z) \leq V(z(0))\}. \quad (29)$$

When $\dot{V}(z) = 0$, we must have $L(x^*, \lambda) = L(x^*, \lambda^*)$ and $L(x, \lambda^*) = L(x^*, \lambda^*)$ by (28). Thus any point $z \in \mathcal{M}$ is an optimal solution of the saddle point problem (8). Lastly, the trick used in the proof of [44, Theorem 15] can be adopted to

show that $z(t)$ eventually converges to a fixed optimal point z^* . By strong duality (Assumption 3), the component x^* of the optimal point z^* is the optimal solution of the OVC problem (1). Thus Theorem 1 is proved.

B. Proof of Theorem 2

Denote $s_1 := [x; \lambda]$, $s_2 := [\xi; \mu]$, and $s := [s_1; s_2]$. The ES-P-PDGD (15) is reformulated in compact form as

$$\dot{s} = \begin{bmatrix} \dot{s}_1 \\ \dot{s}_2 \end{bmatrix} = \begin{bmatrix} g_1(s_1, s_2) \\ \frac{1}{\epsilon}(-s_2 + g_2(t, s_1)) \end{bmatrix} := g(t, s), \quad (30)$$

where the function $g_1(s_1, s_2)$ captures the dynamics (15a)-(15c), and function $g_2(t, s_1)$ is given by

$$g_2 := \begin{bmatrix} \left(\frac{2}{a} v_j(x + a \sin(\omega t)) \sin(\omega_n t) \right)_{n \in [N], j \in \mathcal{M}} \\ (v_j(x + a \sin(\omega t)))_{j \in \mathcal{M}} \end{bmatrix}, \quad (31)$$

where the first part and the second part are associated with the dynamics (15d) of ξ and (15e) of μ , respectively.

The following Lemma 2 states the average map for the function $g_2(t, s_1)$, which is proved in Appendix C.

Lemma 2. *The average of function $g_2(t, s_1)$ is given by*

$$g_2^{\text{av}}(s_1) := \frac{1}{T} \int_0^T g_2(t, s_1) dt = \ell(s_1) + \mathcal{O}(a), \quad (32)$$

where $\ell(s_1) := \begin{bmatrix} \left(\frac{\partial v_j(x)}{\partial x_n} \right)_{n \in [N], j \in \mathcal{M}} \\ (v_j(x))_{j \in \mathcal{M}} \end{bmatrix}$, and T is the minimum common period of the sinusoidal signals $\sin(\omega t)$.

We analyze the stability of the system (30) via averaging theory and singular perturbation theory, which is divided into the following three steps.

Step 1) *Construct a compact set to study the behavior of system (30) restricted to it.*

To apply averaging theory and singular perturbation theory, it requires that the considered trajectories stay within predefined compact sets. Without loss of generality, we consider the compact set $[(\hat{\mathcal{A}} + \Delta \mathbb{B}) \cap \hat{\mathcal{Z}}] \times \Delta \mathbb{B}$ for the initial condition $s(0)$ and any desired $\Delta > 0$. Here, \mathbb{B} denotes a closed unit ball of appropriate dimension, and $\hat{\mathcal{A}} + \Delta \mathbb{B}$ denotes the union of all sets obtained by taking a closed ball of radius Δ around each point in the saddle point set $\hat{\mathcal{A}}$.

According to Theorem 1, there exists a class- \mathcal{KL} function β such that for any initial condition $z(0) \in \hat{\mathcal{Z}}$, the trajectory $z(t)$ of the P-PDGD (9) with the feasible set $\hat{\mathcal{X}}$ satisfies

$$\|z(t)\|_{\hat{\mathcal{A}}} \leq \beta(\|z(0)\|_{\hat{\mathcal{A}}}, t), \quad \forall t \geq 0. \quad (33)$$

Without loss of generality, we assume the desired convergence precision $\nu \in (0, 1)$. Using the β function in (33), we define the set

$$\mathcal{F} := \left\{ s_1 \in \hat{\mathcal{Z}} : \|s_1\|_{\hat{\mathcal{A}}} \leq \beta \left(\max_{p \in \hat{\mathcal{A}} + \Delta \mathbb{B}} \|p\|_{\hat{\mathcal{A}}}, 0 \right) + 1 \right\}, \quad (34)$$

which is compact. Due to the boundedness of \mathcal{F} , there exists a positive constant M_1 such that $\mathcal{F} \subset M_1 \mathbb{B}$. Since $\ell(s_1)$ (defined in Lemma 2) is continuous by Assumption 2, there exists a positive constant $M_2 > \Delta$ such that $\|\ell(s_1)\| + 1 \leq M_2$

whenever $\|s_1\| \leq M_1$. We then study the behavior of system (30) **restricted to evolve in the compact set** $\mathcal{F} \times M_2\mathbb{B}$.

Step 2) Study the stability properties of the average system of the original system (30).

By definition (14), the sinusoidal signals in system (30) are given by $\sin(\frac{2\pi}{\varepsilon_\omega} \kappa_n t)$ for $n \in [N]$. For sufficiently small ε_ω , system (30), evolving in $\mathcal{F} \times M_2\mathbb{B}$, is in standard form for the application of averaging theory. By Lemma 2, we derive the autonomous **average system** of system (30), which is given by (35) (evolving in $\mathcal{F} \times M_2\mathbb{B}$):

$$\dot{\mathbf{y}} = \begin{bmatrix} \dot{\mathbf{y}}_1 \\ \dot{\mathbf{y}}_2 \end{bmatrix} = \frac{1}{T} \int_0^T \mathbf{g}(t, \mathbf{y}) dt = \begin{bmatrix} \mathbf{g}_1(\mathbf{y}_1, \mathbf{y}_2) \\ \frac{1}{\varepsilon}(-\mathbf{y}_2 + \ell(\mathbf{y}_1) + \mathcal{O}(a)) \end{bmatrix} \quad (35)$$

where $\mathbf{y} := [\mathbf{y}_1; \mathbf{y}_2]$ takes the same form as $\mathbf{s} := [s_1; s_2]$.

To analyze the average system (35), we can first ignore the small $\mathcal{O}(a)$ -perturbation by setting $a = 0$. Thus the resultant system is in the standard form for the application of singular perturbation theory [45] with the slow dynamics of \mathbf{y}_1 and fast dynamics of \mathbf{y}_2 . As $\varepsilon \rightarrow 0^+$, we freeze the slow state \mathbf{y}_1 , and the **boundary layer system** of the average system (35) with $a = 0$ in the time scale $\tau = t/\varepsilon$ is

$$\frac{d\mathbf{y}_2}{d\tau} = -\mathbf{y}_2 + \ell(\mathbf{y}_1), \quad (36)$$

which is a linear time-invariant system with the unique equilibrium point $\mathbf{y}_2^* = \ell(\mathbf{y}_1)$. As a result, the associated **reduced system** is derived as

$$\dot{\mathbf{y}}_1 = \mathbf{g}_1(\mathbf{y}_1, \ell(\mathbf{y}_1)), \quad (37)$$

which is precisely the P-PDGD (9). By Theorem 1 and [36, Theorem 2], it follows that as $\varepsilon \rightarrow 0^+$, the set $\hat{A} \times M_2\mathbb{B}$ is semi-globally practically asymptotically stable (SGPAS) for the average system (35) with $a = 0$. Then by the structural robustness results for ordinary differential equations with continuous right-hand sides [39, Proposition A.1], the set $\hat{A} \times M_2\mathbb{B}$ is also SGPAS for the average system (35) as $(\varepsilon, a) \rightarrow 0^+$, which is stated as Lemma 3.

Lemma 3. *Given the precision ν , there exists $\varepsilon^* > 0$ such that for any $\varepsilon \in (0, \varepsilon^*)$, there exists $a^* > 0$ such that for any $a \in (0, a^*)$, with initial condition $\mathbf{y}(0) \in [(\hat{A} + \Delta\mathbb{B}) \cap \hat{\mathcal{Z}}] \times \Delta\mathbb{B}$, the solution $\mathbf{y}(t)$ of the average system (35) satisfies that for all $t \geq 0$,*

$$\|\mathbf{y}_1(t)\|_{\hat{A}} \leq \beta(\|\mathbf{y}_1(0)\|_{\hat{A}}, t) + \frac{\nu}{2}. \quad (38)$$

The proof of Lemma 3 is provided in Appendix D.

Step 3) Link the stability property of the average system (35) to the stability property of the original system (30).

Since the set $\hat{A} \times M_2\mathbb{B}$ is SGPAS for the average system (35) as $(\varepsilon, a) \rightarrow 0^+$, by averaging theory for perturbed systems [39, Theorem 7], it directly obtains that for each pair of (ε, a) inducing the bound (38), there exists $\varepsilon_\omega^* > 0$ such that for any $\varepsilon_\omega \in (0, \varepsilon_\omega^*)$, the solution $\mathbf{s}(t)$ of the original system (30) restricted to $\mathcal{F} \times M_2\mathbb{B}$ satisfies

$$\|\mathbf{s}_1(t)\|_{\hat{A}} \leq \beta(\|\mathbf{s}_1(0)\|_{\hat{A}}, t) + \nu, \quad \forall t \geq 0. \quad (39)$$

The completeness of solution \mathbf{s} for the original system (30) is guaranteed by taking M_2 sufficiently large.

Thus Theorem 2 is proved.

C. Proof of Lemma 2

We first consider the integration on the first part of $\mathbf{g}_2(t, \mathbf{s}_1)$. By the Taylor expansion of $v_j(\cdot)$, each component of this integration is ($\forall j \in \mathcal{M}, n \in [N]$)

$$\begin{aligned} & \frac{1}{T} \int_0^T \frac{2}{a} v_j(\mathbf{x} + a \sin(\omega t)) \sin(\omega_n t) dt \\ &= \frac{1}{T} \int_0^T \frac{2}{a} [v_j(\mathbf{x}) + a \nabla v_j(\mathbf{x})^\top \sin(\omega t) + \mathcal{O}(a^2)] \sin(\omega_n t) dt \\ &= \frac{1}{T} \int_0^T 2 \sum_{i=1}^N \frac{\partial v_j(\mathbf{x})}{\partial x_i} \sin(\omega_i t) \sin(\omega_n t) dt + \mathcal{O}(a) \\ &= \frac{\partial v_j(\mathbf{x})}{\partial x_n} \frac{1}{T} \int_0^T 2 \sin(\omega_n t)^2 dt + \mathcal{O}(a) = \frac{\partial v_j(\mathbf{x})}{\partial x_n} + \mathcal{O}(a). \end{aligned}$$

As for the integration on the second part of $\mathbf{g}_2(t, \mathbf{s}_1)$, similarly, each component of this integration is ($\forall j \in \mathcal{M}$)

$$\begin{aligned} & \frac{1}{T} \int_0^T v_j(\mathbf{x} + a \sin(\omega t)) dt \\ &= \frac{1}{T} \int_0^T v_j(\mathbf{x}) + a \nabla v_j(\mathbf{x})^\top \sin(\omega t) + \mathcal{O}(a^2) dt \\ &= v_j(\mathbf{x}) + \mathcal{O}(a^2). \end{aligned}$$

Combining these two parts, Lemma 2 is proved.

D. Proof of Lemma 3

By the arguments of singular perturbation and structural robustness (right above Lemma 3), it follows that the bound (38) holds for all $t \in [0, T_{\mathbf{y}})$, where $[0, T_{\mathbf{y}})$ denotes the maximal time interval of existence of solution \mathbf{y} .

We further show that the solution \mathbf{y} of the average system (35) exists for an unbounded time domain by the following lemma 4, which follows a special case of [46, Lemma 5].

Lemma 4. *Let $M_2 > 0$ be given and $e : \mathbb{R}_+ \rightarrow M_2\mathbb{B}$. Then for any $k > 0$, the set $M_2\mathbb{B}$ is forward invariant for the dynamics $\dot{\mathbf{s}}_2 = k(-\mathbf{s}_2 + e(t))$.*

By the construction of \mathcal{F} (34), we obtain $\mathbf{y}_1(t) \in \text{int}(\mathcal{F})$ for all $t \in [0, T_{\mathbf{y}})$. Moreover, by setting a^* sufficiently small such that $\|\mathcal{O}(a)\| < 1$ for any $a \in (0, a^*)$, it follows that $\|\mathbf{y}_1(t)\| \leq M_1$ and $\|\ell(\mathbf{y}_1(t)) + \mathcal{O}(a)\| < M_2$ for all $t \in [0, T_{\mathbf{y}})$. By Lemma 4, it implies that $\mathbf{y}_2(t) \in \text{int}(M_2\mathbb{B})$ for all $t \geq 0$. Hence, the solution $\mathbf{y}(t) \in \text{int}(\mathcal{F} \times M_2\mathbb{B})$ for all $t \geq 0$, and has an unbounded time domain, i.e., $T_{\mathbf{y}} \rightarrow +\infty$.

REFERENCES

- [1] H. Sun, Q. Guo, J. Qi, and et al., "Review of challenges and research opportunities for voltage control in smart grids," *IEEE Trans. Power Syst.*, vol. 34, no. 4, pp. 2790–2801, 2019.
- [2] W. Zheng, W. Wu, B. Zhang, and Y. Wang, "Robust reactive power optimisation and voltage control method for active distribution networks via dual time-scale coordination," *IET Generation, Transmission & Distribution*, vol. 11, no. 6, pp. 1461–1471, 2017.

- [3] B. A. Robbins, H. Zhu, and A. D. Domínguez-García, "Optimal tap setting of voltage regulation transformers in unbalanced distribution systems," *IEEE Trans. Power Syst.*, vol. 31, no. 1, pp. 256–267, 2016.
- [4] B. A. Robbins and A. D. Domínguez-García, "Optimal reactive power dispatch for voltage regulation in unbalanced distribution systems," *IEEE Trans. Power Syst.*, vol. 31, no. 4, pp. 2903–2913, 2016.
- [5] G. Qu and N. Li, "Optimal distributed feedback voltage control under limited reactive power," *IEEE Trans. Power Syst.*, vol. 35, no. 1, pp. 315–331, 2020.
- [6] H. J. Liu, W. Shi, and H. Zhu, "Hybrid voltage control in distribution networks under limited communication rates," *IEEE Trans. Smart Grid*, vol. 10, no. 3, pp. 2416–2427, 2019.
- [7] H. Zhu and H. J. Liu, "Fast local voltage control under limited reactive power: Optimality and stability analysis," *IEEE Trans. Power Syst.*, vol. 31, no. 5, pp. 3794–3803, 2016.
- [8] N. Li, G. Qu, and M. Dahleh, "Real-time decentralized voltage control in distribution networks," in *52nd Annual Allerton Confer. on Commun., Control, and Computing (Allerton)*, 2014, pp. 582–588.
- [9] J. Zhang, Z. Chen, C. He, Z. Jiang, and L. Guan, "Data-driven-based optimization for power system var-voltage sequential control," *IEEE Trans. Ind. Informat.*, vol. 15, no. 4, pp. 2136–2145, 2019.
- [10] H. Zhang, J. Zhou, Q. Sun, J. M. Guerrero, and D. Ma, "Data-driven control for interlinked ac/dc microgrids via model-free adaptive control and dual-droop control," *IEEE Trans. Smart Grid*, vol. 8, no. 2, pp. 557–571, 2017.
- [11] C. Mugnier, K. Christakou, J. Jatón, M. De Vivo, M. Carpita, and M. Paolone, "Model-less/measurement-based computation of voltage sensitivities in unbalanced electrical distribution networks," in *2016 Power Systems Computation Conference (PSCC)*, 2016, pp. 1–7.
- [12] H. Xu, A. D. Domínguez-García, V. V. Veeravalli, and P. W. Sauer, "Data-driven voltage regulation in radial power distribution systems," *IEEE Trans. Power Syst.*, vol. 35, no. 3, pp. 2133–2143, 2020.
- [13] W. Wang, N. Yu, Y. Gao, and J. Shi, "Safe off-policy deep reinforcement learning algorithm for volt-var control in power distribution systems," *IEEE Trans. Smart Grid*, vol. 11, no. 4, pp. 3008–3018, 2020.
- [14] Y. Zhang, X. Wang, J. Wang, and Y. Zhang, "Deep reinforcement learning based volt-var optimization in smart distribution systems," *IEEE Trans. Smart Grid*, vol. 12, no. 1, pp. 361–371, 2021.
- [15] S. Wang, J. Duan, D. Shi, C. Xu, H. Li, R. Diao, and Z. Wang, "A data-driven multi-agent autonomous voltage control framework using deep reinforcement learning," *IEEE Trans. Power Syst.*, vol. 35, no. 6, pp. 4644–4654, 2020.
- [16] H. Liu and W. Wu, "Two-stage deep reinforcement learning for inverter-based volt-var control in active distribution networks," *IEEE Trans. Smart Grid*, pp. 1–1, 2020.
- [17] X. Chen, G. Qu, Y. Tang, S. Low, and N. Li, "Reinforcement learning for decision-making and control in power systems: Tutorial, review, and vision," *arXiv preprint arXiv:2102.01168*, 2021.
- [18] Y. Chen, A. Bernstein, A. Devraj, and S. Meyn, "Model-free primal-dual methods for network optimization with application to real-time optimal power flow," in *2020 American Control Conference (ACC)*, 2020, pp. 3140–3147.
- [19] K. B. Ariyur and M. Krstić, *Real Time Optimization by Extremum Seeking Control*. Wiley Online Library, 2003.
- [20] M. Ye and G. Hu, "Distributed extremum seeking for constrained networked optimization and its application to energy consumption control in smart grid," *IEEE Trans. Control Syst. Technol.*, vol. 24, no. 6, pp. 2048–2058, 2016.
- [21] M. D. Sankur, R. Dobbe, A. von Meier, and D. B. Arnold, "Model-free optimal voltage phasor regulation in unbalanced distribution systems," *IEEE Trans. Smart Grid*, vol. 11, no. 1, pp. 884–894, 2020.
- [22] X. Li, Y. Li, and J. E. Seem, "Maximum power point tracking for photovoltaic system using adaptive extremum seeking control," *IEEE Trans. Control Syst. Technol.*, vol. 21, no. 6, pp. 2315–2322, 2013.
- [23] D. B. Arnold, M. Negrete-Pincetic, M. D. Sankur, D. M. Auslander, and D. S. Callaway, "Model-free optimal control of var resources in distribution systems: An extremum seeking approach," *IEEE Trans. Power Syst.*, vol. 31, no. 5, pp. 3583–3593, 2016.
- [24] H. Nazaripouya, H. R. Pota, C. Chu, and R. Gadh, "Real-time model-free coordination of active and reactive powers of distributed energy resources to improve voltage regulation in distribution systems," *IEEE Trans. Sustain. Energy*, vol. 11, no. 3, pp. 1483–1494, 2020.
- [25] J. Johnson, A. Summers, R. Darbali-Zamora, J. Hernandez-Alvidrez, J. Quiroz, D. Arnold, and J. Anandan, "Distribution voltage regulation using extremum seeking control with power hardware-in-the-loop," *IEEE J. Photovolt.*, vol. 8, no. 6, pp. 1824–1832, 2018.
- [26] A. D. Flaxman, A. T. Kalai, and H. B. McMahan, "Online convex optimization in the bandit setting: gradient descent without a gradient," *arXiv preprint cs/0408007*, 2004.
- [27] C. Manzie and M. Krstic, "Extremum seeking with stochastic perturbations," *IEEE Trans. Autom. Control*, vol. 54, no. 3, pp. 580–585, 2009.
- [28] A. R. Teel and D. Popovic, "Solving smooth and nonsmooth multivariable extremum seeking problems by the methods of nonlinear programming," in *Proc. of American Control Conference*, pp. 2394–2399, 2001.
- [29] S. Khong, D. Netic, Y. Tan, and C. Manzie, "Unified frameworks for sampled-data extremum seeking control: Global optimisation and multi-unit systems," *Automatica*, no. 49, pp. 2720–2733, 2013.
- [30] J. I. Poveda and A. R. Teel, "A robust event-triggered approach for fast sampled-data extremization and learning," *IEEE Trans. Autom. Control*, no. 10, pp. 4949–4964, 2017.
- [31] X.-B. Gao, "Exponential stability of globally projected dynamic systems," *IEEE Trans. Neural Netw.*, vol. 14, no. 2, pp. 426–431, 2003.
- [32] A. Nagurny and D. Zhang, *Projected Dynamical Systems and Variational Inequalities with Applications*. Springer Science & Business Media, 2012, vol. 2.
- [33] Y. Zhu, W. Yu, G. Wen, and G. Chen, "Projected primal-dual dynamics for distributed constrained nonsmooth convex optimization," *IEEE Trans. Cybern.*, vol. 50, no. 4, pp. 1776–1782, 2020.
- [34] P. Bansode, V. Chinde, S. Wagh, R. Pasumathy, and N. Singh, "On the exponential stability of projected primal-dual dynamics on a riemannian manifold," *arXiv preprint arXiv:1905.04521*, 2019.
- [35] H. K. Khalil and J. W. Grizzle, *Nonlinear Systems*, 3rd ed. Prentice hall Upper Saddle River, NJ, 2002.
- [36] W. Wang, A. Teel, and D. Nešić, "Analysis for a class of singularly perturbed hybrid systems via averaging," *Automatica*, vol. 48, no. 6, pp. 1057–1068, 2012.
- [37] G. Qu and N. Li, "On the exponential stability of primal-dual gradient dynamics," *IEEE Contr. Syst. Lett.*, vol. 3, no. 1, pp. 43–48, 2018.
- [38] M. Farivar, L. Chen, and S. Low, "Equilibrium and dynamics of local voltage control in distribution systems," in *52nd IEEE Conference on Decision and Control*, 2013, pp. 4329–4334.
- [39] J. I. Poveda and N. Li, "Robust hybrid zero-order optimization algorithms with acceleration via averaging in time," *Automatica*, vol. 123, p. 109361, 2021.
- [40] R. D. Zimmerman, C. E. Murillo-Sánchez, and R. J. Thomas, "Matpower: Steady-state operations, planning and analysis tools for power systems research and education," *IEEE Trans. Power Syst.*, vol. 26, no. 1, pp. 12–19, Feb. 2011.
- [41] M. Grant and S. Boyd, "CVX: Matlab software for disciplined convex programming, version 2.1," <http://cvxr.com/cvx>, Mar. 2014.
- [42] A. Ruszczyński, *Nonlinear Optimization*. Princeton university press, 2011.
- [43] F. H. Clarke, *Optimization and Nonsmooth Analysis*. Wiley: Society Series of Monographs and Advanced Texts, SIAM, 1990.
- [44] N. Li, C. Zhao, and L. Chen, "Connecting automatic generation control and economic dispatch from an optimization view," *IEEE Control Netw. Syst.*, vol. 3, no. 3, pp. 254–264, 2015.
- [45] A. R. Teel, L. Moreau, and D. Netic, "A unified framework for input-to-state stability in systems with two time scales," *IEEE Trans. Autom. Control*, vol. 48, no. 9, pp. 1526–1544, 2003.
- [46] S. Park, N. Martins, and J. Shamma, "Payoff dynamics model and evolutionary dynamics model: Feedback and convergence to equilibria," *arXiv:1903.02018v4*, 2020.